23rd ABCM International Congress of Mechanical Engineering
December 6-11, 2015, Rio de Janeiro, RJ, Brazil

STRESS AND STRAIN DISTRIBUTION OF AN ANISOTROPIC BONE

Lucas Lisbôa Vignoli
Mechanical Eng. Dept., Pontifical Catholic University of Rio de Janeiro, PUC-Rio, Marques de São Vicente Street, 225, Gávea, Rio de Janeiro, RJ, Brazil, 22451-900
lucaslvig@gmail.com

Paulo Pedro Kenedi[1,2]
[1]DEMEC - Departamento de Engenharia Mecânica - CEFET/RJ - Av. Maracanã, 229 -Maracanã - RJ - CEP 20271-110 - Brazil
[2]PPEMM- Programa de Pós-Graduação em Engenharia Mecânica e Tecnologia de Materiais - CEFET/RJ - Av. Maracanã, 229 - Maracanã - RJ - CEP 20271-110 – Brazil
paulo.kenedi@cefet-rj.br

Abstract. *In this work two analytical models were proposed to biomechanical applications, using solid mechanics and theory of elasticity, to estimate the principal stress and strain distribution, and respective principal angles, at a bone medial cross section external surface. To validate the proposed analytical models, a finite element (FE) model of a long bone, with real geometry and same applied static loads, is provided. For the analytical solid mechanics model, the bone material was assumed as isotropic and for the analytical model based in theory of elasticity the bone material was set as orthotropic, defined according to the radial, tangential and longitudinal directions. Although real human femur geometry has a quite irregular shape, the analyzed medial bone cross section was modeled as a hollow circular pattern. Both analytical and F,E, models results showed that the principal stress and strain angles were compatible with actual dominant osteonal bone range angles.*

Keywords: *bone, femur, anisotropy.*

1. INTRODUCTION

Bone is a live tissue, it can grow, self-repair when damaged, and continuously being renewed by internal remodeling events. Also bones are non-homogeneous, porous and anisotropic, Doblaré *et al*. (2004). It is accepted that the main path of bone remodeling process overlaps the principal stresses angles. Although this process makes it stronger, it makes bone tissue quite anisotropic. Both analytical and F.E. approaches are used to model a femur submitted to static loads, using two constitutive bone relationships: isotropic and orthotropic. The principal stress/strain and the correspondent principal angles are accessed. These results are compared with bone osteonal angles.

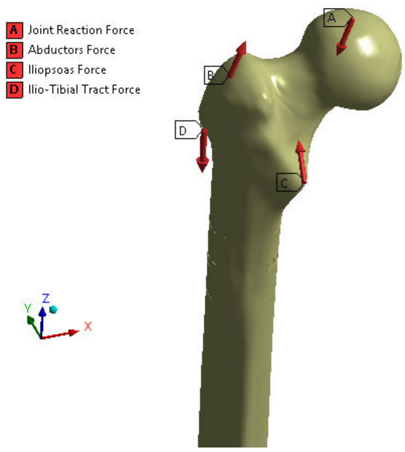

Figure 1: Human femur static loading model.

In this work is used a four forces loading model, adapted from Taylor *et al*. (1996) to generate the static loading condition at proximal femur, as schematically shown at Fig.1. It proposes to verify if the Petrtýl *et al*. (1996) and Cowin and Hart (1990) proposition that the principal stress angles at a medial external surface of a human femur are compatible with the dominant osteonal angles.

Table 1 shows the elastic mechanical properties obtained, in technical literature Kenedi and Riagusoff, (2015) and Korsa and Mares, (2012), respectively, for isotropic and orthotropic bone materials, used by analytical and numerical models at the application example. Only the independent constants are represented (two for isotropic and nine for orthotropic), once the others can be readily obtained.

Table 1: Elastic mechanical properties.

Material Properties	Isotropic used at Kenedi and Riagusoff, (2015)	Orthotropic used at Korsa and Mares, (2012)
E (GPa)	20	-
E_1 (GPa)	-	12
E_2 (GPa)	-	13.4
E_3 (GPa)	-	20
ν	0.235	-
ν_{12}	-	0.376
ν_{13}	-	0.222
ν_{23}	-	0.234
G_{12} (GPa)	-	4.53
G_{13} (GPa)	-	5.61
G_{23} (GPa)	-	6.23

At the next section the analytical models expressions will be presented.

2. ANALYTICAL MODELS

Bone is from macroscopic point of view, a non-homogeneous, porous and anisotropic tissue, Doblaré *et al*. (2004). Although at human femur can coexist cortical and trabecular bone tissues, at medial cross section the cortical bone prevails, which is followed by this work. The force and moments components at a medial cross-section and the coordinates systems used are shown at Fig.2.

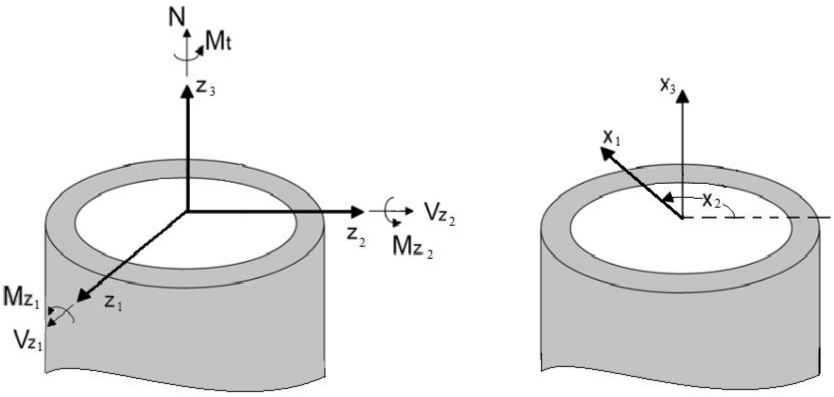

(a) (b)

Figure 2: (a) Force and moments components at a medial cross-section with the cartesian coordinate system and (b) medial cross-section with the cylindrical coordinate system.

Two different models will be presented and compared: the analytical solid mechanics model, Kenedi and Riagusoff (2015) for an isotropic femur and the analytical theory of elasticity model, Lekhniskii (1981) for an orthotropic femur. See also Vignoli (2014).

The summation of the contributions of forces and moments acting in a specific medial bone cross section are:

$$V_{z_1} = \sum_{i=1}^{4} V_i^{z_1} \qquad V_{z_2} = \sum_{i=1}^{4} V_i^{z_2} \qquad N = \sum_{i=1}^{4} V_i^{z_3}$$

$$M_{z_1} = \sum_{i=1}^{4} M_i^{z_1} \qquad M_{z_2} = \sum_{i=1}^{4} M_i^{z_2} \qquad M_t = \sum_{i=1}^{4} M_i^{z_3} \tag{1}$$

Where $V_i^{z_1}$, $V_i^{z_2}$ and $V_i^{z_3}$, where *i* ranges from 1 to 4, and represents the force components shown at Fig. 1. Also $M_i^{z_1}$, $M_i^{z_2}$ and $M_i^{z_3}$ where *i* ranges from 1 to 4, represents the moments components generated by the forces shown at Fig. 1.

2.1 Isotropic Model (ISOM)

The isotropic materials have only two independent mechanical elastic constants, the Young modulus E and the Poisson ratio ν. The ISOM expressions are presented:

The cortical axial stress σ_{33}^{axial} is, Crandall (1978):

$$\sigma_{33}^{axial} = \frac{N}{A} \qquad \text{where} \qquad A = 2\pi t\left(r_o - \frac{t}{2}\right) \tag{2}$$

Where A is the cortical area, r_o is the outer radius and t is the cortical tissue thickness.

The cortical bending stress components, $\sigma_{33}^{bend_1}$ and $\sigma_{33}^{bend_2}$ are, Crandall (1978):

$$\sigma_{33}^{bend_1} = \frac{M_{z_1}}{I} z_2 \qquad \sigma_{33}^{bend_2} = -\frac{M_{z_2}}{I} z_1$$
$$z_1 = z_1(\gamma) = -r_o(\gamma)\cos(\gamma) \quad z_2 = z_2(\gamma) = r_o(\gamma)\sin(\gamma) \quad I = \frac{\pi}{4}\left(r_o^4 - r_i^4\right) \tag{3}$$

where $z_1(\gamma)$ and $z_2(\gamma)$ are, respectively, the perpendicular distances from axis z_1 and z_2 to external cortical bone surfaces, I_{z_1} and I_{z_2} are second moment of area, respectively, about x and y axis. r_i is the inner radius.

The cortical torsional stress $\tau_{23}^{torsion}$ is Crandall (1978):

$$\tau_{23}^{torsion} = \frac{M_t}{J} x_1 \qquad \text{where} \qquad J = \frac{\pi}{2}\left(r_o^4 - r_i^4\right) \tag{4}$$

where J is the polar moment of inertia.

The transverse shear stress of cortical components, τ_{13}^{trans} and τ_{23}^{trans} are Crandall (1978):

$$\tau_{13}^{trans} = \tau_{13}^{trans}(\gamma) = \frac{V_{z_1} Q_{z_2}(\gamma)}{I t_{z_2}(\gamma)} \qquad \tau_{23}^{trans} = \tau_{23}^{trans}(\gamma) = \frac{V_{z_2} Q_{z_1}(\gamma)}{I t_{z_1}(\gamma)}$$
$$t_{z_1}(\gamma) = 2\sqrt{r_o^2 - \left(z_2(\gamma)\right)^2}, \quad for \ r_i \le |z_2| \le r_o \qquad t_{z_2}(\gamma) = 2\sqrt{r_o^2 - \left(z_1(\gamma)\right)^2}, \quad for \ r_i \le |z_1| \le r_o \tag{5}$$
$$Q_{z_1}(\gamma) = \frac{2}{3}\left(r_o^2 - \left(z_2(\gamma)\right)^2\right)^{3/2}, \quad for \ r_i \le |z_2| \le r_o \qquad Q_{z_2}(\gamma) = \frac{2}{3}\left(r_o^2 - \left(z_1(\gamma)\right)^2\right)^{3/2}, \quad for \ r_i \le |z_1| \le r_o$$

where $Q_{z_1}(\gamma)$ and $Q_{z_2}(\gamma)$, are first moments of area, $t_{z_1}(\gamma)$ and $t_{z_2}(\gamma)$ are thicknesses.

2.2 Anisotropic Model (ANISOM)

The orthotropic materials have nine independent mechanical elastic constants, three Young moduli, three shear moduli and three Poisson ratios, Lekhniskii (1981). For orthotropic materials, the stiffness matrix can be expressed as

$$C = \begin{bmatrix} \frac{1}{E_1} & -\frac{\nu_{21}}{E_2} & -\frac{\nu_{31}}{E_3} & 0 & 0 & 0 \\ -\frac{\nu_{12}}{E_1} & \frac{1}{E_2} & -\frac{\nu_{32}}{E_3} & 0 & 0 & 0 \\ -\frac{\nu_{13}}{E_1} & -\frac{\nu_{23}}{E_2} & \frac{1}{E_3} & 0 & 0 & 0 \\ 0 & 0 & 0 & \frac{1}{G_{23}} & 0 & 0 \\ 0 & 0 & 0 & 0 & \frac{1}{G_{13}} & 0 \\ 0 & 0 & 0 & 0 & 0 & \frac{1}{G_{12}} \end{bmatrix} \tag{6}$$

Where, E_i is the Modulus of elasticity at directions x_i; G_{ij} is the Shear Modulus acting at the face x_i and at directions x_j; ν_{ij} is the Poisson ratio at the face x_i and at directions x_j.

The ANISOM expressions are shown is sequence. Some variables used in original Lekhnitskii (1981) are modified for clarity sake. The only simplification assumption of this model is not considering the transverse forces effect, which for a long bone like a human femur is quite reasonable.

The normal stresses produced by axial force are, Lekhniskii (1981):

$$\sigma_{11}^{axial}=\frac{Nh}{T}\left[1-\frac{1-\rho^{k+1}}{1-\rho^{2k}}\left(\frac{x_1}{r_o}\right)^{k-1}-\frac{1-\rho^{k-1}}{1-\rho^{2k}}\rho^{k+1}\left(\frac{x_1}{r_o}\right)^{-k-1}\right] \tag{7.a}$$

$$\sigma_{22}^{axial}=\frac{Nh}{T}\left[1-\frac{1-\rho^{k+1}}{1-\rho^{2k}}k\left(\frac{x_1}{r_o}\right)^{k-1}+\frac{1-\rho^{k-1}}{1-\rho^{2k}}k\rho^{k+1}\left(\frac{x_1}{r_o}\right)^{-k-1}\right] \tag{7.b}$$

$$\sigma_{33}^{axial}=\frac{N}{T}-\frac{Nh}{TC_{33}}\left[C_{13}+C_{23}-\frac{1-\rho^{k+1}}{1-\rho^{2k}}\left(C_{13}+kC_{23}\right)\left(\frac{x_1}{r_o}\right)^{k-1}-\frac{1-\rho^{k-1}}{1-\rho^{2k}}\left(C_{13}+kC_{23}\right)\rho^{k+1}\left(\frac{x_1}{r_o}\right)^{-k-1}\right] \tag{7.c}$$

Where r_o is the external radius, r_i is the internal radius, $\rho = r_i/r_o$ is the ration between the internal and the external radius and h, T and k are additional parameters created to get a more compact expressions and are defined at Appendix. The stress distribution produced by the internal resultant bending moment in global coordinate z_1 are, Lekhniskii (1981):

$$\sigma_{11}^{bend_1}=-\frac{M_{z_1}r_og}{K}\left[\left(\frac{x_1}{r_o}\right)-\frac{1-\rho^{m+2}}{1-\rho^{2m}}\left(\frac{x_1}{r_o}\right)^{m-1}+\frac{1-\rho^{m-2}}{1-\rho^{2m}}\rho^{m+2}\left(\frac{x_1}{r_o}\right)^{-m-1}\right]\sin\left(x_2\right) \tag{8.a}$$

$$\sigma_{22}^{bend_1}=-\frac{M_{z_1}r_og}{K}\left[3\left(\frac{x_1}{r_o}\right)-\frac{1-\rho^{m+2}}{1-\rho^{2m}}(1+m)\left(\frac{x_1}{r_o}\right)^{m-1}+\frac{1-\rho^{m-2}}{1-\rho^{2m}}(1-m)\rho^{m+2}\left(\frac{x_1}{r_o}\right)^{-m-1}\right]\sin\left(x_2\right) \tag{8.b}$$

$$\sigma_{33}^{bend_1}=\left\{-\frac{M_{z_1}x_1}{K}-\frac{M_{z_1}r_og}{KC_{33}}\left[(C_{13}+3C_{23})\left(\frac{x_1}{r_o}\right)-\frac{1-\rho^{m+2}}{1-\rho^{2m}}(C_{13}+(1+m)C_{23})\left(\frac{x_1}{r_o}\right)^{m-1}+\frac{1-\rho^{m-2}}{1-\rho^{2m}}(C_{13}+(1-m)C_{23})\rho^{m+2}\left(\frac{x_1}{r_o}\right)^{-m-1}\right]\right\}\sin\left(x_2\right) \tag{8.c}$$

$$\tau_{12}^{bend_1}=\frac{M_{z_1}r_og}{K}\left[\left(\frac{x_1}{r_o}\right)-\frac{1-\rho^{m+2}}{1-\rho^{2m}}\left(\frac{x_1}{r_o}\right)^{m-1}-\frac{1-\rho^{m-2}}{1-\rho^{2m}}\rho^{m+2}\left(\frac{x_1}{r_o}\right)^{-m-1}\right]\cos\left(x_2\right) \tag{8.d}$$

Where m, g and K are additional parameters created to get a more compact equation and are defined at the Appendix. The stress distribution produced by the internal resultant bending moment in global coordinate z_2 are, Lekhniskii (1981):

$$\sigma_{11}^{bend_2}=\frac{M_{z_2}r_og}{K}\left[\left(\frac{x_1}{r_o}\right)-\frac{1-\rho^{m+2}}{1-\rho^{2m}}\left(\frac{x_1}{r_o}\right)^{m-1}+\frac{1-\rho^{m-2}}{1-\rho^{2m}}\rho^{m+2}\left(\frac{x_1}{r_o}\right)^{-m-1}\right]\cos\left(x_2\right) \tag{9.a}$$

$$\sigma_{22}^{bend_2}=-\frac{M_{z_2}r_og}{K}\left[3\left(\frac{x_1}{r_o}\right)-\frac{1-\rho^{m+2}}{1-\rho^{2m}}(1+m)\left(\frac{x_1}{r_o}\right)^{m-1}+\frac{1-\rho^{m-2}}{1-\rho^{2m}}(1-m)\rho^{m+2}\left(\frac{x_1}{r_o}\right)^{-m-1}\right]\cos\left(x_2\right) \tag{9.b}$$

$$\sigma_{33}^{bend_2}=\left\{-\frac{M_{z_2}x_1}{K}+\frac{M_{z_2}r_og}{KC_{33}}\left[(C_{13}+3C_{23})\left(\frac{x_1}{r_o}\right)-\frac{1-\rho^{m+2}}{1-\rho^{2m}}(C_{13}+(1+m)C_{23})\left(\frac{x_1}{r_o}\right)^{m-1}+\frac{1-\rho^{m-2}}{1-\rho^{2m}}(C_{13}+(1-m)C_{23})\rho^{m+2}\left(\frac{x_1}{r_o}\right)^{-m-1}\right]\right\}\cos\left(x_2\right) \tag{9.c}$$

$$\tau_{12}^{bend_2}=-\frac{M_{z_2}r_og}{K}\left[\left(\frac{x_1}{r_o}\right)-\frac{1-\rho^{m+2}}{1-\rho^{2m}}\left(\frac{x_1}{r_o}\right)^{m-1}-\frac{1-\rho^{m-2}}{1-\rho^{2m}}\rho^{m+2}\left(\frac{x_1}{r_o}\right)^{-m-1}\right]\sin\left(x_2\right) \tag{9.d}$$

The shear stress produced by torsional moment is presented at (10) in global coordinate z_3.

$$\tau_{23}^{torsion}=\frac{M_t}{J}x_1 \tag{10}$$

Where J is the polar moment of area.

At next section the principal stress and strain direction, with their respective angles, are estimated.

2.3 Principal Stress/Strain and Principal angles

As it is a linear elastic study, the stress can be computed using the Superposition Method, Crandall (1978):

$$\sigma_{11}=\sigma_{11}^{axial}+\sigma_{11}^{bend_1}+\sigma_{11}^{bend_2} \qquad \sigma_{22}=\sigma_{22}^{axial}+\sigma_{22}^{bend_1}+\sigma_{22}^{bend_2} \qquad \sigma_{33}=\sigma_{33}^{axial}+\sigma_{33}^{bend_1}+\sigma_{33}^{bend_2} \tag{11.a}$$

$$\tau_{23}=\tau_{23}^{torsion}+\tau_{23}^{trans} \qquad \tau_{13}=\tau_{13}^{trans} \qquad \tau_{12}=\tau_{12}^{bend_1}+\tau_{12}^{bend_2} \tag{11.b}$$

For a generic load, the stresses and strains can be analyzed in a 3x3 symmetric matrix:

$$T = \begin{bmatrix} \sigma_{11} & \tau_{12} & \tau_{13} \\ \tau_{12} & \sigma_{22} & \tau_{23} \\ \tau_{13} & \tau_{23} & \sigma_{33} \end{bmatrix} \qquad e = \begin{bmatrix} \varepsilon_{11} & \gamma_{12} & \gamma_{13} \\ \gamma_{12} & \varepsilon_{22} & \gamma_{23} \\ \gamma_{13} & \gamma_{23} & \varepsilon_{33} \end{bmatrix} \tag{12}$$

The eigenvalues and eigenvectors of these matrices have a special physical meaning, the eigenvalues are the principal stresses and principal strains and the eigenvectors are their respective angles. Mathematically, the eigenvalues can be calculated as

$$\left| T_{ij} - t\delta_{ij} \right| = 0 \qquad \left| e_{ij} - s\delta_{ij} \right| = 0 \tag{13}$$

Where t and s are the principal stresses and strains and δ_{ij} is the Kronecker delta. Once the eigenvalues are obtained, the eigenvectors can be computed as

$$\left[T_{ij} - t\delta_{ij} \right]\left[l_i \right] = 0 \quad , \quad \left[e_{ij} - s\delta_{ij} \right]\left[m_i \right] = 0 \tag{14}$$

At bone surface, where the plane stress condition takes place, the principal stresses and strains can be also calculated as

$$t_1 = \frac{\sigma_{22} + \sigma_{33}}{2} + \left[\left(\frac{\sigma_{22} - \sigma_{33}}{2} \right)^2 + \left(\tau_{23} \right)^2 \right] \tag{15.a}$$

$$t_2 = 0 \tag{15.b}$$

$$t_3 = \frac{\sigma_{22} + \sigma_{33}}{2} - \left[\left(\frac{\sigma_{22} - \sigma_{33}}{2} \right)^2 + \left(\tau_{23} \right)^2 \right] \tag{15.c}$$

$$s_1 = \frac{\varepsilon_{22} + \varepsilon_{33}}{2} + \left[\left(\frac{\varepsilon_{22} - \varepsilon_{33}}{2} \right)^2 + \left(\frac{\gamma_{23}}{2} \right)^2 \right] \tag{15.d}$$

$$s_2 = \varepsilon_{11} \tag{15.e}$$

$$s_3 = \frac{\varepsilon_{22} + \varepsilon_{33}}{2} - \left[\left(\frac{\varepsilon_{22} - \varepsilon_{33}}{2} \right)^2 + \left(\frac{\gamma_{23}}{2} \right)^2 \right] \tag{15.f}$$

And the slope of the principal directions on the external surface are

$$\Phi_{stress} = \frac{1}{2} a\tan\left(\frac{2\tau_{23}}{\sigma_{22} - \sigma_{33}} \right) \quad , \quad \Phi_{strain} = \frac{1}{2} a\tan\left(\frac{\gamma_{23}}{\varepsilon_{22} - \varepsilon_{33}} \right) \tag{16}$$

Despite the three principal strains are different of zero along the bone external surface, γ_{12} and γ_{13} are equal to zero. In other words, there is no distortion caused by shear effect acting on the radial direction, thus the direction of s_2 coincides to the radial direction, as shown at Eq. (15.e).

At next section the Finite Element Approach will be detailed.

3. FINITE ELEMENT APPROACH

A numerical model was developed using the F.E. ANSYS software. The static loading is composed by the joint reaction force and three principal muscles forces, as shown at Fig. 1

3.1 FE Model

The bone distal region was fixed to ensure equilibrium requirements. To extract the results, one path, on the medial cross section along the bone external surface, was created as shown in Fig.3.a. The purple arrow indicates the path orientation.

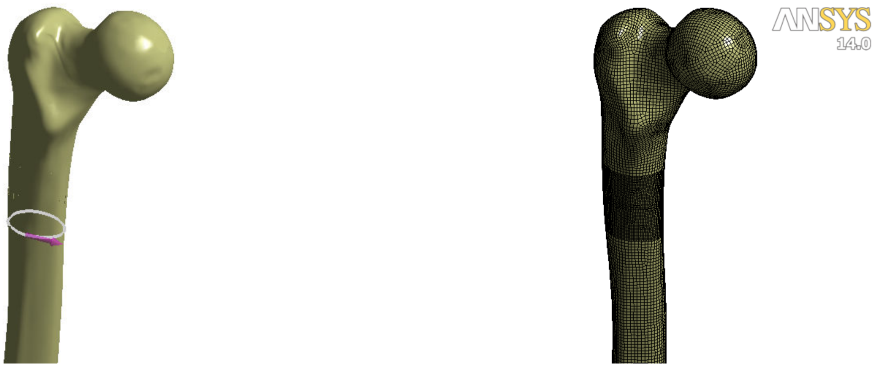

(a) (b)

Figure 3**:** (a) Path created to extract the results and (b) Mesh used on the F.E. simulations.

Figure 3.b shows the mesh used at the human femur bone. At medial section, where the path is located, it was refined to access more accurate results. As the bone has a quite irregular shape, it was used SOLID186 and SOLID187 elements, which exhibits a quadratic displacement behavior, Lee (2012). Table 2 shows the loading forces utilized and geometric constants (note that P_1 , P_2 , P_3 and P_4 are applied, respectively, at points *A*, *B*, *C* and *D* of Fig.1).

Table 2: Loading forces and geometric constants. (* approximate measure)

Joint reaction force	P_1(N)	(–1,062; -130; -2,800)
Abductors force	P_2 (N)	(430; 0; 1,160)
Iliopsoas force	P_3 (N)	(78; 560; 525)
Ilio-Tibial Tract force	P_4 (N)	(0; 0; -1,200)
P_1 point of application	A (mm)	(50.7; -2.7; 133)
P_2 point of application	B (mm)	(-13.5; -6.5; 115)
P_3 point of application	C (mm)	(18.8; -29.3; 58.7)
P_4 point of application	D (mm)	(-24.6; -4.2; 83)
cross section centroid	(mm)	(0.8; 2.4; -25)
R_e (external radius)	(mm)*	15.5
R_i (internal radius)	(mm)*	7.6

Note that the numerical simulation was done using the orthotropic mechanical properties.

3.2 FE Results

In this section the results of the numerical F.E. model, described on the previous section, and the analytical model (ANISOM) are compared. The principal stresses and principal strains are presented using path approach, $0° \leq \theta \leq 360°$, to make possible a more precise results presentation. To validate the analytical model, as well as the hypotheses adopted, the results of the principal stresses and strains for both analytical and numeric models are plotted at Fig. 4. Note that it was utilized the more generic case of anisotropy covered by this work, the orthotropic, for both analytical and numeric F.E. models.

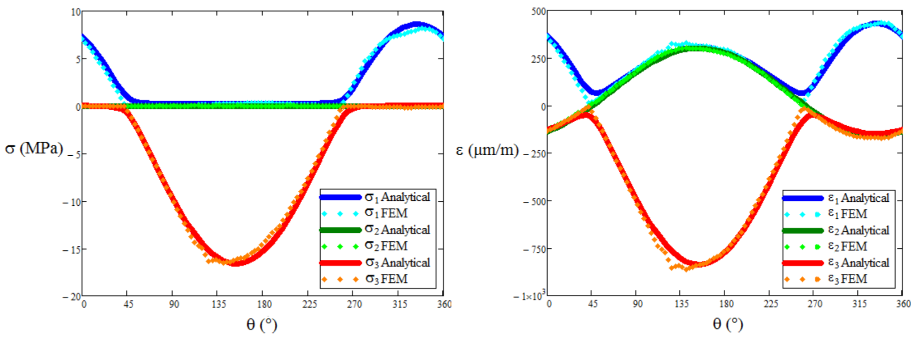

Figure 4: Comparison between analytical (ANISOM) and F.E. models for principal: (a) stress and (b) strain.

Where the indexes 1, 2 and 3 refers to the maximum, intermediate and minimum principal stress/strains. Fig. 4 shows that the geometry simplification assumed during the analytical approach do not affected significantly the analytical model performance when compared to F.E. approach. Indeed the analytical model (ANISOM) performance can be considered satisfactory. At next section the analytical models will be compared.

4. MODELS COMPARISON

The properties presented in Table 1 are used to compare the effect of the level of anisotropy in stress and strains distributions at a medial cross section external surface path. At Figures 5.a and 5.b, the analytical models principal stresses and strains are compared.

Note that the path is along a free external surface, thus the intermediate principal stresses is always zero, the intermediate principal strain do not interfere on the principal strain vector direction at the x_2-x_3 plane.

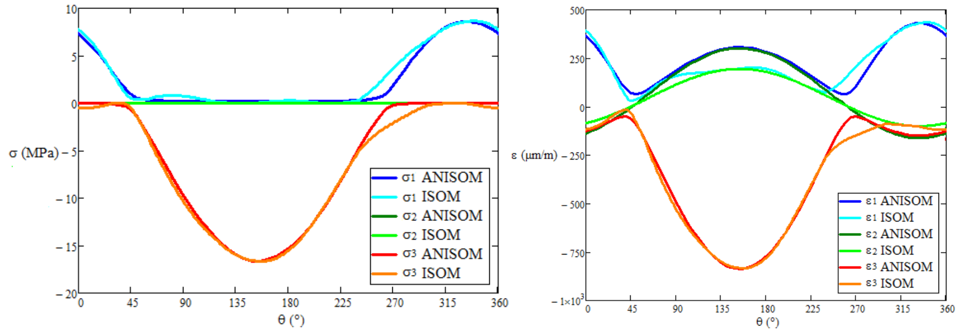

(a) (b)

Figure 5: Comparison between analytical models: (a) Principal stresses and (b) principal strains.

At Fig. 5, the principal stresses and strains values are slightly different for isotropic and orthotropic models. Although the anisotropy do not influences significantly the stress and strains distribution, its importance becomes clear when the principal angles are analyzed at Fig.6.

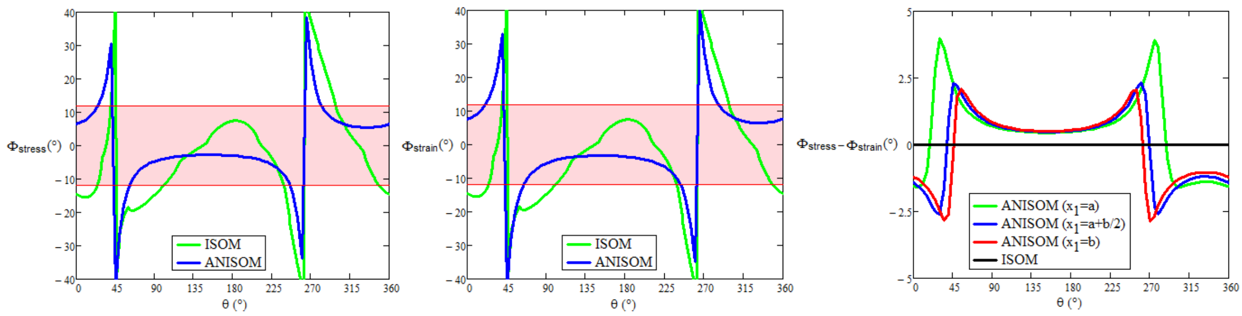

(a) (b) (c)

Figure 6: Principal angles directions: (a) Stress, (b) strain and (c) the difference between them.

The red band represents the experimental results related by Petrtýl *et al.* (1996) as the experimental slope of bone lamellae range. The analytical results shown at Fig. 6 revels that both principal stress and strain angles have some differences related with the level of anisotropy: isotropic or orthotropic. Fig. 6.c shows the variation between principal stress and strain angles according to the radial position. Note that Fig. 6 shows two angles, around 45° and 260°, where there are an abrupt change of angles behavior.

5. CONCLUSIONS

The ISOM is a simple approach model based in solid mechanics to estimate the stresses distribution at bone medial cross section external surface, as showed by Kenedi and Riagusoff (2015), it only recognize isotropic materials. The ANISOM, that uses theory of elasticity applied for cylindrically orthotropic materials, Lekhniskii (1981), recognizes the orthotropic nature of bone tissue. Analyzing both principal stress and strain angles, for both analytical models, most of the angle results remain inside the Fig. 6.a and 6.b shaded area, with the exception of angles around $\theta = 45°$ and $\theta = 260°$, which is compatible with dominant osteonal range angles related by Petrtýl *et al.* (1996).

6. ACKNOWLEDGEMENTS

The authors thank the Brazilian foundation CNPq and the PUC-Rio for financial support.

7. REFERENCES

Cowin, S.C. and Hart, R.T. (1990). Errors in the orientation of the principal stress axes if bone tissue is modeled as isotropic, J. Biomech., Technical Note, (23), issue 4, pp. 349-352.

Crandall, S.H., Dahl, N.C. and Lardner, T.J. (1978). An Introduction to the Mechanics of Solids, Second Edition with SI units, McGraw Hill International Editions.

Doblaré, M., García J. M. and Gómez, M. J. (2004). Modeling bone tissue fracture and healing: a review, Engineering Fracture Mechanics, (71), pp. 1809-1840.

Kenedi, P.P., Riagusoff, I.I.T.(2015). Stress development at human femur by muscle forces, J Braz. Soc. Mech. Sci. Eng., 37(1), pp. 31-43.

Korsa, R., Mares, T.(2012). Numerical Identification of Orthotropic Coefficients of the Lamella of a Bone's Osteon, Bulletin of Applied Mechanics, 8(31), pp. 45-53.

Lee, H. H. (2012). Finite Element Simulations with ANSYS Workbench 14, SDC Publications.

Lekhniskii, S.G. (1981). Theory of elasticity of an anisotropic body, Mir.

Petrtýl, M., Herf, J. and Fiala, P. (1996). Spatial Organization of the Haversian Bone in Man, J. Biomech., (29), No. 2, pp. 161-169.

Taylor, M.E., Tanner, K.E., Freeman, M.A.R. and Yettram, A.L. (1996). Stress and strain distribution within the intact femur: compression or bending?, Med. Eng. Phys., 18: 2, pp. 122-131.

Vignoli, L.L., (2014). Análise de Ossos Longos Anisotrópicos, 21th National Congress of Mechanical Engineering Students – CREEM 2014. Rio de Janeiro, Brazil.

8. RESPONSIBILITY NOTICE

The authors are the only responsible for the printed material included in this paper.

9. APPENDIX

Constants used to presents expressions in a more compact form.

$$\beta_{ij} = C_{ij} - \frac{C_{i3}C_{i3}}{C_{33}}$$

$$g = \frac{C_{23} - C_{13}}{\beta_{11} + 2\beta_{12} + 2\beta_{66} - 3\beta_{22}}$$

$$h = \frac{C_{23} - C_{13}}{\beta_{11} - \beta_{22}}$$

$$k = \left(\frac{\beta_{11}}{\beta_{12}}\right)^{\frac{1}{2}}$$

$$m = \left(1 + \frac{\beta_{11} + 2\beta_{12} + 2\beta_{66}}{\beta_{22}}\right)^{\frac{1}{2}}$$

$$K = \left\{\frac{\pi r_o^4}{4}\left(1-\rho^4\right) - \frac{\pi r_o^4 g}{C_{33}}\left[\left(1-\rho^4\right)\left(\frac{C_{13}+3C_{23}}{4}\right) - \frac{\left(1-\rho^{2m}\right)^2}{\left(1-\rho^{2m}\right)}\left(\frac{C_{13}+(1+m)C_{23}}{m+2}\right) - \frac{\left(1-\rho^{m-2}\right)^2}{\left(1-\rho^{2m}\right)}\rho^4\left(\frac{C_{13}+(1-m)C_{23}}{m-2}\right)\right]\right\}$$

$$T = \left\{\pi r_o^2\left(1-\rho^2\right) + \frac{2\pi h r_o^2}{C_{33}}\left[\left(1-\rho^2\right)\left(\frac{C_{13}+C_{23}}{2}\right) - \left(1-\rho^{k+1}\right)^2\left(\frac{C_{13}+kC_{23}}{k+1}\right) - \left(1-\rho^{k-1}\right)^2\rho^2\left(\frac{C_{13}-kC_{23}}{k-1}\right)\right]\right\}$$